Applied Physics B (2021) 127:111
https://doi.org/10.1007/s00340-021-07663-0

Applied Physics B
Lasers and Optics

Generation of frequency comb and its dependence on gain suppression in directly modulated semiconductor laser

Alaa Mahmoud[1] · **Moustafa Ahmed**[2,3]

Received: 14 January 2021 / Accepted: 6 July 2021 / Published online: 12 July 2021

Abstract
This paper presents a theoretical study on the generation of optical frequency combs (OFCs) using direct modulation of semiconductor laser. Influence of gain suppression on characteristics of the generated OFCs is investigated. The study includes intensive and comprehensive investigations of the temporal and spectral characteristics of the generated OFCs as a function of the gain suppression over a wide range of the bias current. We report on generation of short optical pulses and large numbers of comb lines with low-power flatness under weak gain suppression and/or strong modulation depth when the laser is biased near the threshold. The influence of gain suppression becomes more robust when the laser is biased far above threshold. By adopting the operating parameters, we predict pulses with 60 ps width and 10 comb lines with 2.1 dB flatness when the gain suppression is ignored. Under strong gain suppression, broader pulses (132 ps width) and only five lines with higher flatness of 4.99 dB could be obtained.

1 Introduction

In recent years, optical frequency comb (OFC) generation has gained considerable attention from researchers because of its wide-ranging applications such as optical arbitrary waveform generation [1], radio-photonics [2], optical communications [3, 4], etc. The essential characteristics required for most of these applications are generating a large number of comb lines with a high degree of flatness together with good linewidth characteristics [5]. This is regardless of the other different comb characteristics needed depending on the application being targeted [6].

Generating OFCs using semiconductor laser is based on three main strategies; namely, traditional mode-locked lasers (MLLs) [7], electro-optic modulators (EOMs) [8] and gain switching (GS) laser [9–14]. Although traditional MLLs can generate high-stability OFCs, they are relatively complicated and costly [7], and do not provide a wavelength tunability due to the fixed comb line spacing, which is decided by the laser cavity length (or the inverse of the round trip time for light propagating in the cavity) [10]. Adjusting the comb line spacing can be obtained using external modulations [15]. In this case, multiple external modulators are required to improve the flatness of the comb, which results in increases the cost and insertion loss [15, 16]. Another method that has recently gained attention is frequency-modulated (FM) mode-locking, which is favorable for many single-section semiconductor lasers with fast gain dynamics [17–21]. In this method, the spatial hole burning effect initially enhances lasing on multiple longitudinal modes with non-equidistant spacing. The four-wave mixing effect can lock the phases of these modes together and equalize the spacing [17]. This approach is preferred for applications requiring high average optical power and quasi-continuous-wave intensity [19]. Although the wavelength portfolio of FM combs is expanding, there are several practical relevance wavelength ranges that have yet to be explored [19]. EOMs method for generating OFCs provide a relatively large number of optical comb lines with easily adjustable spacing, but they suffer from significant insertion loss from the modulators, and need extra optical components that increase the complexity and cost of the transmitter [6, 10]. On the other hand, compared with previous techniques, generating OFCs by GS technique based on direct modulation of semiconductor laser has advantages of simple implementation, low cost, stability,

✉ Alaa Mahmoud
alaa.abutaleb@lira.bsu.edu.eg

[1] Laser Institute for Research and Applications (LIRA), Beni-Suef University, Beni-Suef, Egypt

[2] Department of Physics, Faculty of Science, King Abdulaziz University, 80203, Jeddah 21589, Saudi Arabia

[3] Department of Physics, Faculty of Science, Minia University, Minia, Egypt

low losses, and flexibility in tuning the frequency spacing of the comb lines (frequency repetition rate) by varying the modulation frequency [6, 10, 11]. Therefore, such a technique has become a focus of research for more interesting applications, such as radio-over-fiber (RoF) technology [22], multi-wavelength sources [23] and multicarrier transmission systems [24]. Moreover, it has been proved as achievable dual-comb spectroscopy by OFCs generated by GS technique [25]. However, generating OFCs by GS technique suffers from a limited bandwidth and large phase noise [26].

Several studies were concerned with enhancing the characteristics of the gain-switched OFCs and improving its spectral quality using external optical injection method [12, 13, 27, 28]. However, this method increases the total cost and needs considerable care to avoid unstable operation induced by external effects like temperature, vibration, polarization, etc. In literature, to the best of our knowledge, only Anandarajah et al. [10] reported on possibility of generation of an OFC without need for external injection via gain switching. The study was concerned with modulation frequencies around the relaxation oscillation frequency of the laser. However, there were insufficient details on influence of the gain-switching conditions and intrinsic nonlinear properties of the laser on the generated OFC [10].

The GS technique based on direct modulation of semiconductor laser is typically accomplished by modulating the semiconductor laser by a sinusoidal RF current in conjunction directly with the bias current to switch on and off the laser gain [11, 13]. Semiconductor lasers modulated with such pulsed pump current, often exhibit damped oscillations (commonly referred to as relaxation oscillations) whose pulse width is significantly shorter than the electrical pulse. These oscillations result from the coupling between electrons and photons through stimulated emission [29, 30]. The idea then is to pick up the first intensity spike of these oscillations, at the beginning of the laser operation, without exciting the next ones by switching off the RF current period [31, 32]. Therefore, single pulses can be generated simply by modulating the semiconductor laser biased below or near the threshold with a large RF current amplitude (i.e., strong modulation depth) [31, 33], to ensure the signal clipping. Ahmed et al. [34] showed that modulating the laser under deep modulation with frequencies around the relaxation oscillation frequency induces pulsed signals with period-doubling.

The characteristics of OFCs generated by GS the laser diode mainly depend on both the amplitude and frequency of the RF current and the bias current [11, 13]. Another intrinsic property of the laser that may control OFCs is the nonlinear gain suppression because it affects the dynamic response of the laser [35]. Gain suppression was proved to suppress the carrier-photon resonance and increase the damping rate of relaxation oscillations and is hence affected to the generation of OFCs [36–38]. Nonlinear gain suppression may be attributed to different physical mechanisms, in particular, spectral hole burning [39], nonlinear absorption [40], carrier diffusion [41] and dynamic carrier heating effects [42, 43].

In this paper we introduce a comprehensive simulation study on the generation of OFCs induced by GS technique basing direct modulation of semiconductor laser by a sinusoidal current signal as a potential comb generation technique. We investigate the generation of OFCs and bring together details on their temporal and spectral characteristics. We present insight into influence of gain suppression on laser dynamics in terms of transient relaxation oscillations, corresponding phase portraits, and small-signal modulation response. Also, we examine impact of gain-switching conditions on the generated OFCs; namely, the bias current and the modulation depth at the important frequency of carrier-photon resonance. The results show that when the laser is biased near the threshold value, short optical pulses and large number of comb lines with low-power flatness are generated at low degree of gain suppression and/or strong modulation depth. Moreover, the influence of gain suppression is more robust when the laser is biased far above threshold value.

2 Theoretical model and simulation method

The dynamics of single-mode semiconductor laser including generation of OFCs are simulated basing on the following pair of rate equations of the photon number $S(t)$ and injected electron number $N(t)$ in a single field mode [44]

$$\frac{\mathrm{d}S}{\mathrm{d}t} = [G - G_{\mathrm{th}}]S + \frac{a\xi}{V}N \tag{1}$$

$$\frac{\mathrm{d}N}{\mathrm{d}t} = \frac{I(t)}{e} - AS - \frac{N}{\tau_s}, \tag{2}$$

where G is the gain per unit time and described as [45]:

$$G = A - BS \tag{3}$$

The coefficient $A = a\xi/V(N - N_g)$ is the linear gain term, while B is the coefficient of nonlinear gain suppression and is given by

$$B = \frac{9}{2}\frac{\pi c}{\varepsilon_o n_a^2 \hbar \lambda_o}\left(\frac{\xi \tau_{\mathrm{in}}}{V}\right)^2 a|R_{\mathrm{cv}}|^2(N - N_s) \tag{4}$$

N_g and N_s are the electron numbers at transparency and that character B, respectively. In Eq. (1), G_{th} is the threshold gain level and is given in terms of the material loss κ, power

reflectivities of the front and back facets (R_f and R_b, respectively), and active region length L as [46]

$$G_{th} = \frac{c}{n_a}\left\{k + \frac{1}{2L}\ln\left(\frac{1}{R_f R_b}\right)\right\} \approx \frac{a\xi}{V}\left(N_{th} - N_g\right), \tag{5}$$

where N_{th} is the electron number at the threshold level. The other parameters in the above equations are defined with their typical values in Table 1.

The direct modulation of SL is described in the rate equations by representing the injection current $I(t)$ in Eq. (2) by the following sinusoidal form.

$$I(t) = I_b\left(1 + m\sin(2\pi f_m t\right), \tag{6}$$

where I_b is the bias current, m is the modulation depth and f_m is the modulation frequency.

Rate Eqs. (1) and (2) are integrated numerically by the 4th-order Runge–Kutta algorithm [47]. The integration time step is set $\Delta t = 5$ ps and the integration is taken over a period of $T = 300$ ns. The time step is short enough to provide a good resolution of the temporal trajectories of $S(t)$. Over a finite period T, the frequency content of the temporal trajectory of $S(t)$ is determined by the fast Fourier transformation (FFT) as [48]

$$S_f = \frac{1}{T}\left|\int_0^T S(t)e^{-j2\pi f\tau}d\tau\right|^2 \cong \sqrt{\frac{\Delta t}{T}}\left|\mathrm{FFT}(S(t))\right|, \tag{7}$$

where f is the Fourier frequency. This frequency spectrum S_f is used to reveal the generated frequency components of the oscillating mode (fundamental, harmonic and sub-harmonic frequencies), which are the comb lines, and to determine their power flatness (power differences between comb lines).

The small-signal modulation response $H_m(f_m)$ at a given modulation frequency f_m with a small sinusoidal perturbation $\Delta I = mI_b$ around I_b is defines as the transfer function from input current modulation to optical output power [49]. Therefore, $H_m(f_m)$ is evaluated as the ratio of the modulated photon number $S_m(f_m)$ to the corresponding non-modulated value $S_m(0)$ and is given by [50]

$$H\left(f_m\right) = \frac{S_m(f_m)}{S_m(0)} = \frac{f_r^2}{\frac{j}{\pi}\Gamma_r f_m + f_r^2 - f_m^2}, \tag{8}$$

where f_r and Γ_r are the relaxation oscillation frequency and the average damping rate of the laser in the transient regime, respectively, and are determined approximately from the small-signal approach as [50]

$$f_r \approx \frac{1}{2\pi}\sqrt{\left(\frac{a\xi}{V}\right)\left[\frac{a\xi\tau_s}{eV}\left(I_b - I_g\right) + BS_b\right]S_b}, \tag{9}$$

$$\Gamma_r \approx \frac{1}{2}\left[\frac{a\xi}{V} + B\right]S_b, \tag{10}$$

where $I_g = eN_g/\tau_s$ is the transparency current, and S_b is the bias component of $S(t)$ and is determined by

Table 1 Definitions and typical values of the FP-InGaAsP laser parameters used in calculations

Parameter	Meaning	Value	Unit
λ_o	Emission wavelength	1.55	μm
a	Deferential gain coefficient	7.9×10^{-12}	m^3s^{-1}
ξ	Field confinement factor in the active layer	0.2	–
V	Volume of the active region	150×10^{-18}	m^3
N_g	Electron number at transparency	1.33×10^8	–
ε_o	Electric permittivity	8.85×10^{-12}	Fm^{-1}
n_a	Refractive index of active region	3.513	–
τ_{in}	Electron intraband relaxation time	0.1	Ps
$\lvert R_{cv}\rvert^2$	Squared absolute value of the dipole moment	9.52×10^{-57}	C^2m^2
N_s	Electron number characterizing gain suppression	1.01×10^8	–
α	Linewidth enhancement factor	4	–
τ_s	Electron lifetime by spontaneous	1	ns
G_{th}	Threshold gain level	2.88×10^{11}	s^{-1}
I_{th}	Threshold current	25	mA
k	Coefficient of material loss	1000	m^{-1}
L	Length of the active region	300	μm
R_f	Front facet reflectivity	0.3	–
R_b	Back facet reflectivity	0.8	–
B_o	Initial gain suppression coefficient	18,885	C^2ms^{-2}

$S_b = (I_b - I_{th})/eG_{th}$ with I_{th} is the threshold current $I_{th} = eN_{th}/\tau_s$.

3 Results and discussion

3.1 Influence of gain suppression on laser dynamics

First, we examine the influence of nonlinear gain suppression on the transient characteristics of free running SL by varying the coefficient of gain suppression B relative to its initial value $B_o = 18{,}885\ C^2m\ s^{-2}$ as calculated via Eq. (4) and using the parameters in Table 1. The modulation depth in this case is canceled ($m = 0$) and hence, the laser is injected only by the dc bias current I_b. Figure 1a, b show typical dynamics of the photon number $S(t)$ during the laser transients under three different values of gain suppression; namely, without gain suppression ($B = 0$), with its initial value ($B = B_o$), and with high degree ($3B_o$), when the laser is biased near and far above the threshold value, $I_b = 1.2I_{th}$ and $3I_{th}$, respectively. Figure 1a indicates that the stimulated emissions are negligible up to 0.65 ns (turn-on delay times). The photon number $S(t)$ and electron $N(t)$ display the transient spikes through the known relaxation damped oscillations before they reach their steady-state values [37, 51]. The figure shows that the relaxation oscillation frequencies are nearly constant at $f_r \sim 2.7$ GHz. The influence of gain suppression appears clearly in the damping rates Γ_r of relaxation oscillations; the increase in B works to strength the damping rates, which agree with the results in [50, 52, 53]. This may be attributed to the nonlinear dependence of the gain on the electron density as reported by Zhao et al. [53] when they derived expressions for the carrier distribution functions accounting for the spectral hole burning. This enhancement in the damping rates shrinks the time instants at which oscillations disappear (setting time of relaxation oscillations). As a numerical example, the oscillations disappear at 6 ns without gain suppression ($B = 0$), while they disappear at 3.5 and 2 ns when B increases to B_o and $3B_o$, respectively. The decrease in these setting times is considered as a desired condition for enhancing the performance of optical communication systems that operate at high bit rates [51]. More details are illustrated in the inset of the Fig. 1a; it is seen that the increase in gain suppression induces a slight increase in the pulse width of the relaxation oscillations. For example, the full width half maximum (FWHM) of the first spike is about 70 ps when $B = 0$ and it broadens to 72 and 85 ps when B increases to B_o and $3B_o$, respectively. These effects are seen clearly in the second spikes.

When the bias current is increased to far above threshold ($I_b = 3I_{th}$), the turn-on delay time is reduced to 0.13 ns, whereas the relaxation oscillation frequency is still constant but increases to 8.9 GHz [see Eq. (9)] with shorter pulses as shown in Fig. 1b. The figure reveals also that the increase in B induces a significant increase in the damping rates. This significant increase in the damping rates at high bias current is in agreement with the findings of Zhao et al. [53] who attributed this to the increase in the nonlinearity of the gain-electron density dependence at high bias levels [also see Eq. (10)]. The inset of Fig. 1(b) illustrates also that the FWHM pulse width of the first spike is about 18.5 ps when $B = 0$ and is broadened to 24 and 37 ps when B is increased to B_o and $3B_o$, respectively. Comparing Fig. 1a, b indicates that the influence of B is more robust at high bias currents, which agrees with the findings in Refs. [35, 38, 50]. Moreover, it can be found that the influence of B on the relaxation oscillation frequencies f_r is almost negligible in both bias

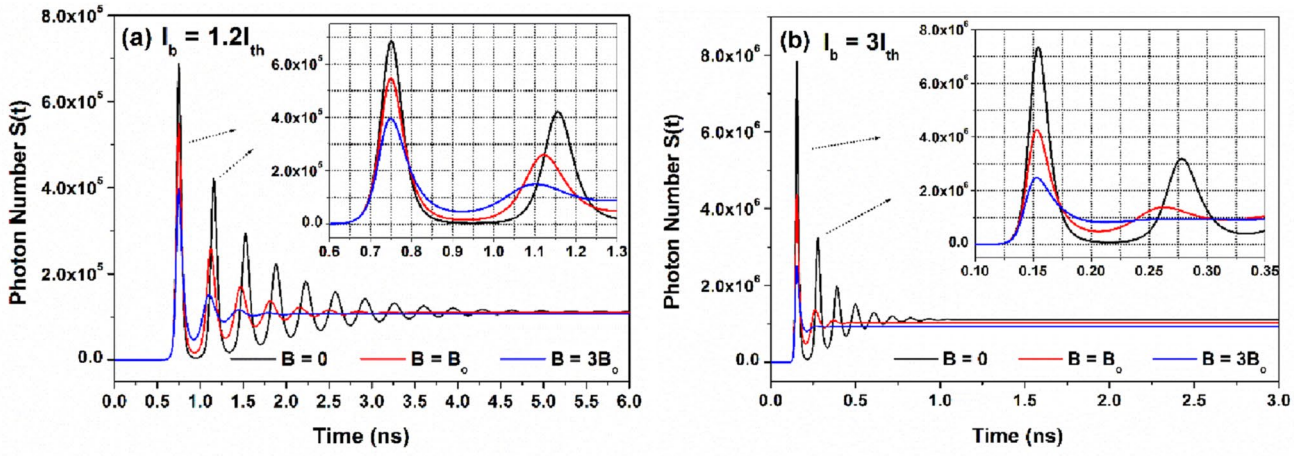

Fig. 1 Transients of photon numbers $S(t)$ with different gain suppression degrees of $B = 0$ (black lines), $B = B_o$ (red lines) and $B = 3B_o$ (blue lines), when bias current I_b is **a** $1.2I_{th}$ and **b** $3I_{th}$

levels in consistence with the findings of Ahmed et al. [50] and Zhao et al. [53].

The transient characteristics of SL can also be understood by looking at the phase-space trajectory of the dynamic variables $S(t)$ and $N(t)$. Figure 2 plots the corresponding phase portrait of the transient characteristics of Fig. 1 to elucidate the effect of B on the correlations among electron and photon numbers. The direction of time evolution is indicated by the arrow in each figure. Figure 2a–f correspond to the condition of $I_b = 1.2I_{th}$ and $3I_{th}$, respectively. For each bias level, B is varied as in Fig. 1 ($B = 0$, B_o and $3B_o$). The figures illustrate that all trajectories are often characterized by a spiral flattened motion towards a fixed point (a stable focus), which is the steady-state value. The intensity of oscillations reduces with the time variation, which is the reason why the phase-space trajectory is converged. The increase in B induces a decrease in the number of loops and the fixed points (focuses) tend to become nodes. This is due to the fact that the electron and photon numbers become more and more out of phase with the increase in B and induces an increase in the damping rates of relaxation oscillations. Our results related to the trajectory shape agree with those plotted by Lingnau et al. [54] when they investigated effect of electron scattering lifetimes on the damping rates of quantum dot lasers. Comparing Fig. 2a–f indicate that there is a decrease in the number of loops resulting from raising I_b from 1.2 to $3I_{th}$, which is an indicator for increasing the damping rates as a function of I_b as confirmed by the results of Fig. 1.

Figure 3a, b plot the small-signal intensity modulation responses $|H_m(f_m)|$ of semiconductor laser as a function of B when $I_b = 1.2I_{th}$ and $3I_{th}$, respectively. The modulation depth in this case is very week ($m = 0.1$). Regardless the influence of B, the figures exhibit clear response peaks at modulation frequency f_m approximately equal to the relaxation oscillation frequency f_r. This indicates a complete synchronized phase between the electron and photon numbers (resonance case). Figure 3a shows that the response peak appears at $f_{m(peak)} \approx f_r = 2.7$ GHz when $I_b = 1.2I_{th}$, while it appears at $f_{m(peak)} \approx f_r = 8.9$ GHz when $I_b = 3I_{th}$ as seen in Fig. 3b. Increasing the gain suppression degree works to reduce the spectrum of $|H_m(f_m)|$. The reduction in $|H_m(f_m)|$ is pronounced around the peaks and is more robust at high bias level ($3I_{th}$) than at low ($1.2I_{th}$), as seen in Fig. 3a, b, respectively. This confirms the fact that the influence of B on the laser characteristics is significant at high bias levels as mentioned in the above discussions. Figure 4 plots variation of the response peak as a function of B/B_o when $I_b = 1.2$ and $3I_{th}$. The figure shows that when B increases from 0 to $3B_o$, the response peak is slightly reduced with 0.24 dB (from 0.47 to 0.23 dB) when $I_b = 1.2I_{th}$, whereas it is significantly reduced with 0.6 dB when $I_b = 3I_{th}$. The figure indicates also that the influence of B is significant when it increases beyond B_o.

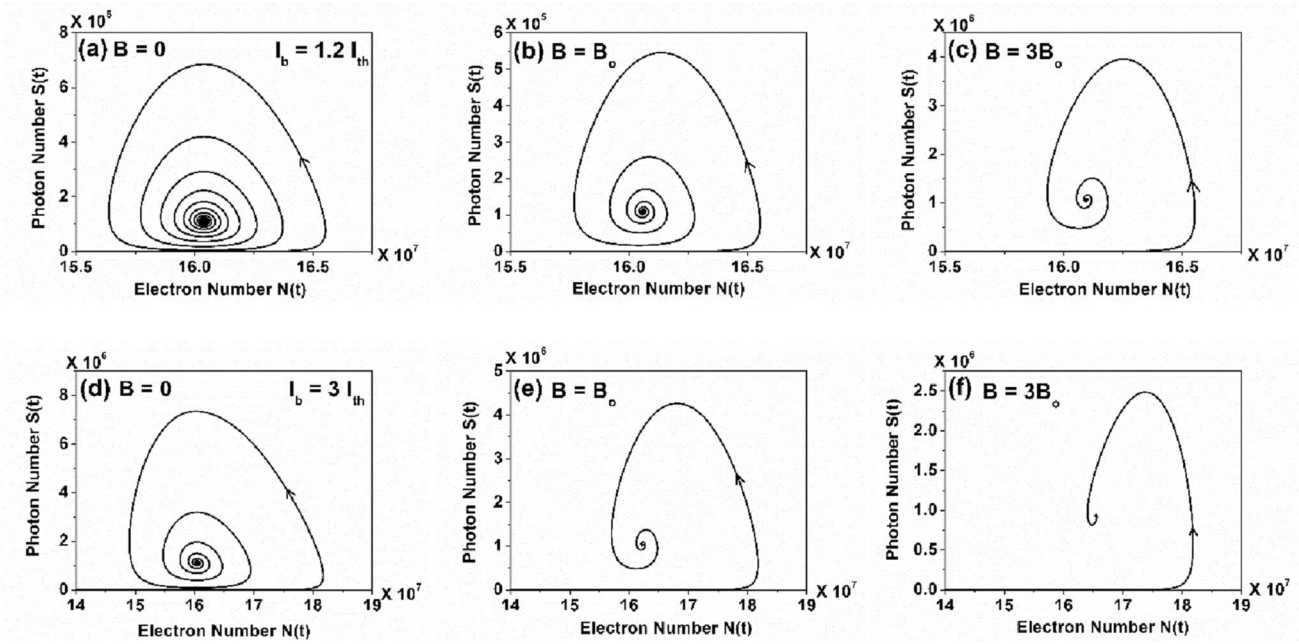

Fig. 2 Phase-space trajectory of (N-S) under different B degrees of 0, B_o and $3B_o$, when **a**–**c** $I_b = 1.2I_{th}$ (upper row) and **d**–**f** $3I_{th}$ (lower row)

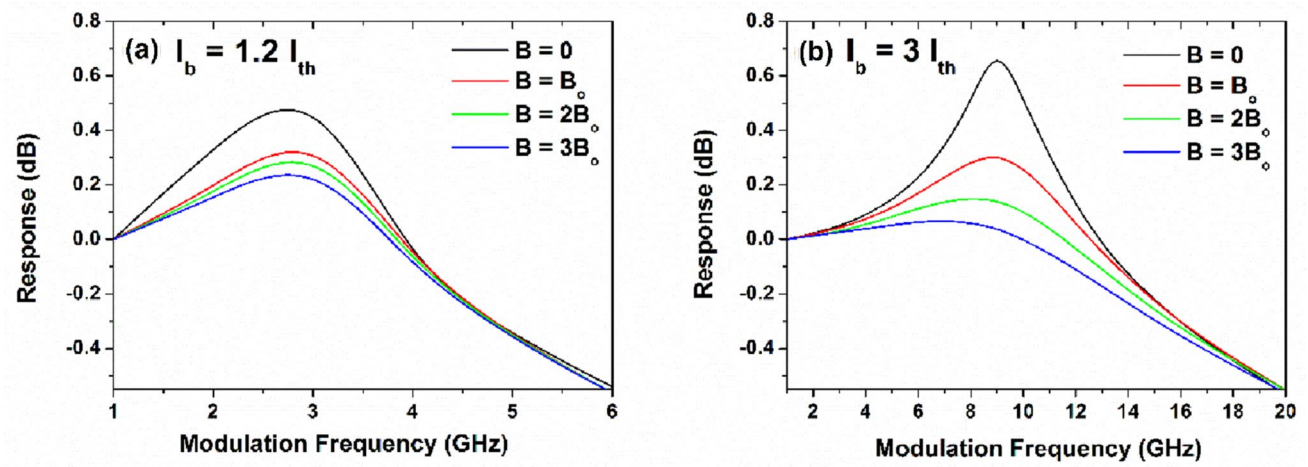

Fig.3 Modulation response under different gain suppression degrees ($B=0$, B_o, $2B_o$ and $3B_o$) when **a** $I_b=1.2I_{th}$ and **b** $I_b=3I_{th}$

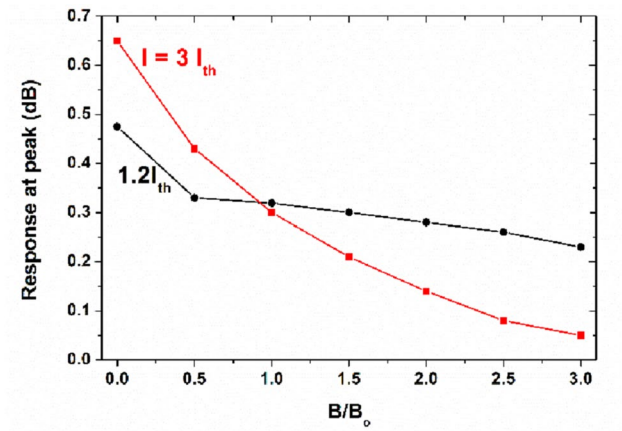

Fig.4 Variation of the response peak as a function of gain suppression degree when $I_b=1.2I_{th}$ (black line) and $3I_{th}$ (red line)

3.2 Influence of gain suppression on the generated OFC characteristics

In this subsection, we investigate in details the suggestion of generation of OFCs by large-signal direct modulation of the investigated semiconductor laser and dependence of their temporal and spectral characteristics on gain suppression. The cavity length of the used laser is constant and the modulation frequency f_m is set to be the relaxation oscillation frequency f_r because this high-frequency regime is rich with nonlinearities. This condition along with strong modulation depth ensures depletion of carrier density when the modulation current goes under the threshold current, which accumulates the lasing photons in the cavity and then emitted when the current goes above threshold (gain-switching of the laser) [11, 13]. The investigations are carried out under the two investigated bias currents of $I_b=1.2I_{th}$ and $3I_{th}$.

Figure 5 displays evolution of the temporal and spectral characteristics of the laser outputs which look like OFCs generated under using three degrees of gain suppression of $B=0$, B_o and $3B_o$. The modulation parameters are set to be $I_b=1.2I_{th}$ and modulation frequency $f_m=f_r=2.7$ GHz with strong modulation depth $m=1$. These modulation parameters ensure clipping the signal with a large quantity of population pulsations [32] and hence induce period-doubling pulses [34]. Figure 5a, c, e (left-hand side column) display the temporal trajectories of the photon numbers $S(t)$ normalized to its time-averaged value (S_{av}) (on the left axis), and the associated injected electron numbers $N(t)$ normalized to its threshold value (N_{th}) (on the right axis). Figure 5b, d, f (right-hand side column) display the corresponding FFT power spectra S_f. Figure 5a shows that when $B=0$, the laser emission appears as intense pulses, each one induces a significant drop in the electron population below the threshold value. Therefore, there is no sufficient population for the production of lasing pulse in the successive period. Thus, one optical pulse appears during two successive periods of the modulation current; a character of period-doubling pulsation. On the other hand, the FFT power spectra reveal several harmonic products as seen in Fig. 5b. The power differences between the fundamental signal (f_m) and these products are commonly called distortions effects. The figure indicates that there are strong sub-harmonics at $f_m/2$ appear together with the higher-order harmonics that appear at multiples of f_m. As a result, 10 comb lines are generated with a power flatness of 2.9 dB and a spacing of 1.35 GHz ($f_m/2$) with spectral width of 12.15 GHz within 2.9 dB of the spectral envelope peak, which in good agreement with the results reported in [11]. These harmonics and sub-harmonics result when the laser resonance is pulled towards this frequency [55, 56]. They may be attributed to lower laser damping rate obtained when gain suppression effect is ignored ($B=0$).

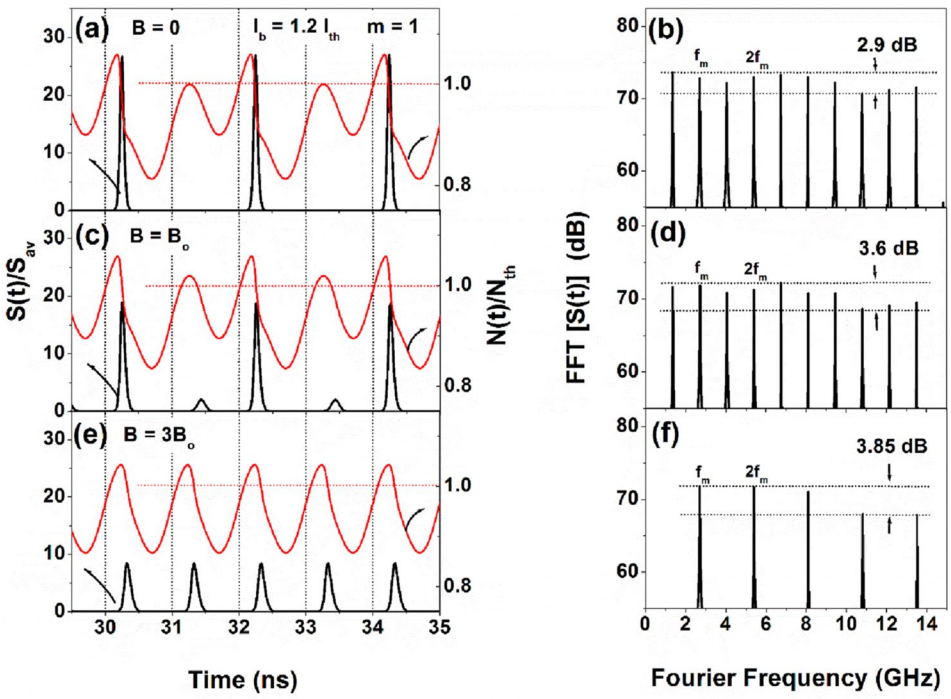

Fig. 5 Temporal and spectral characteristics of laser output when $I_b = 1.2I_{th}$ and $m = 1$ with $f_m = f_r = 2.7$ GHz when **a**, **b** $B = 0$, **c**, **d** B_o and **e**, **f** $3B_o$. The left-hand side column (**a**, **c**, **e**) plots the temporal trajectories of $S(t)$ normalized to average values (black lines on left axis), and the temporal trajectories of $N(t)$ normalized to its threshold values (red lines on right axis). The right-hand side column (**b**, **d**, **f**) plots the corresponding FFT power spectrum S_f

The relation between damping rate and distortion effects was investigated in the experiments of Hemery et al. [57] even at week modulation depth.

With the increase of gain suppression to $B = B_o$, the harmonic distortion is little released with the appearance of other weaker pulses in the repetition of the half-harmonic $f_r/2$, as illustrated in Fig. 5c. That is non-equal two pulses repeats every two periods as a character of distorted period-doubling pulsation. The weaker pulse is generated due to a slight increase in the electron numbers over its threshold value as shown in the right axis of Fig. 5c. Figure 5d confirms the slight decrease in the distortion effects, which seems to be due to an increase in the damping rate. The laser still generates 10 comb lines with $f_m/2$ spacing (1.35 GHz), but the power flatness is increased to 3.6 dB.

The further increase of gain suppression to $3B_o$ induces generation of period-1 pulsation, the pulses have the same height and are generated in repetition of the modulation frequency $f_m = f_r$, as shown in Fig. 5e. In this case, the number of electrons exceeds the threshold value and equals for each period as shown in the right axis of the figure. This condition is often a desired operation for optical communication systems [57]. The corresponding power spectrum is illustrated in Fig. 5f, which indicates that the strong degree of gain suppression results in releasing the power spectrum from sub-harmonics. The spectrum is characterized only with the higher harmonics at multiples of f_m. As a result, only five comb lines are generated with a spacing of $f_m = 2.7$ GHz, and power flatness as large as 3.85 dB. It is worth noting that the increase in B induces a decrease in the pulse height (photon number) and a significant increase in the pulse width due to the reduction in population pulsation. As a numerical example, the FWHM pulse width is 67 ps when $B = 0$ and spreads to 80 and 119 ps when B increases to B_o and $3B_o$, respectively.

Figure 6 displays the evolution of the temporal and spectral characteristics of the OFCs generated at three degrees of gain suppression ($B = 0$, B_o and $3B_o$) when $I_b = 3I_{th}$ and $f_m = f_r = 8.9$ GHz with strong modulation depth $m = 2.8$. The increase in the bias current requires an increase in the modulation depth to ensure the signal clipping and hence gain-switching laser. The temporal trajectories of both $S(t)$ and the associated $N(t)$ are plotted in Fig. 6a, c, e (left-hand side column), whereas the corresponding FFT power spectra are plotted in Fig. 6b, d, f (right-hand side column). Although the temporal and spectral characteristics of the generated OFCs are almost similar to those of Fig. 5, the comb lines generated under these modulation conditions are with higher power flatness and at larger spaces, in addition to generated wider pulses. The frequency spacing of the comb lines (frequency repetition rate) therefore can be controlled by the modulation frequency f_m; the frequency spacing increases by increasing the modulation frequency. Figure 6b displays 10 comb lines with a power flatness of 3.98 dB and a spacing of 4.45 GHz ($f_m/2$) when $B = 0$. The maximum spectral width of the generated OFC, in this case, reaches 40 GHz within 3.98 dB of the spectral envelope peak, which in good agreement with the results reported in [11]. When B increases to B_o, the laser still generate 10 comb lines with a spacing of 4.45 GHz, but the power flatness increased to 4.75 dB as

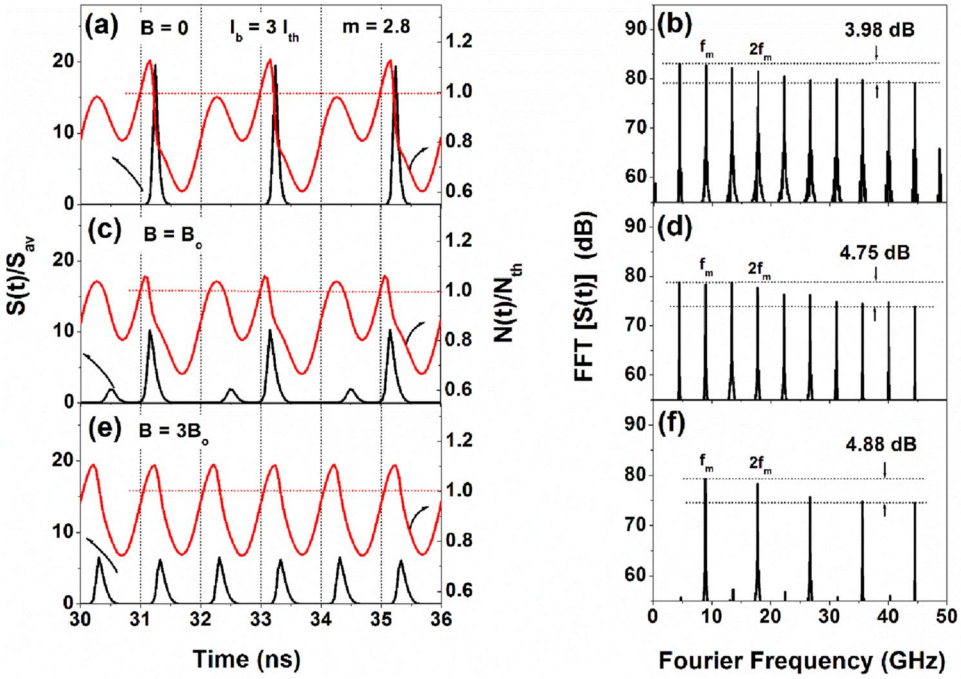

Fig. 6 Temporal and spectral characteristics of laser output when $I_b = 3I_{th}$ and $m = 2.8$ with $f_m = f_r = 8.9$ GHz when **a**, **b** $B = 0$, **c**, **d** B_o and **e**, **f** $3B_o$. The left-hand side column (**a**, **c**, **e**) plots the temporal trajectories of $S(t)$ normalized to average values (black lines on left axis), and temporal trajectories of $N(t)$ normalized to its threshold values (red lines on right axis). The right-hand side column (**b**, **d**, **f**) plots the corresponding FFT power spectrum S_f

seen in Fig. 6d. At high degree of gain suppression ($3B_o$), the sub-harmonics disappear and only the harmonic distortions remain as seen in Fig. 6f. Therefore, there are five comb lines separated with $f_m = 8.9$ GHz with higher power flatness of 4.88 dB. Regarding pulse widths, it is noticed a clear spread in the pulse widths with increase of B as illustrated in Fig. 6a, c, e. As a numerical example, the FWHM pulse width is about 85 ps at $B = 0$ and spreads to 141 and 146 ps when B increases to B_o and $3B_o$, respectively.

Influence of gain suppression on the signal distortion and the generated combs is investigated in more details in Fig. 7a, b, which plot the number of the generated comb lines and their power flatness under three modulation depths for gain switching of $m = 0.5$, 1 and 2.8 when $I_b = 1.2$ and $3I_{th}$, respectively. The number of comb lines is located below each point in the figures. Both figures indicate increase of power flatness with the increase of B. This power flatness decreases with the increase of the modulation depth. In Fig. 7a, when B increases from 0 to $3B_o$ the number of comb lines is ten and decreases to 4 when $m = 0.5$ and to 5 when $m = 1.0$. On the other hand the case of $I_b = 3I_{th}$ in Fig. 7b, the number is almost unchanged with the increase of B. That is, it could be concluded in general that larger number of comb lines with lower-power flatness is generated at lower degree

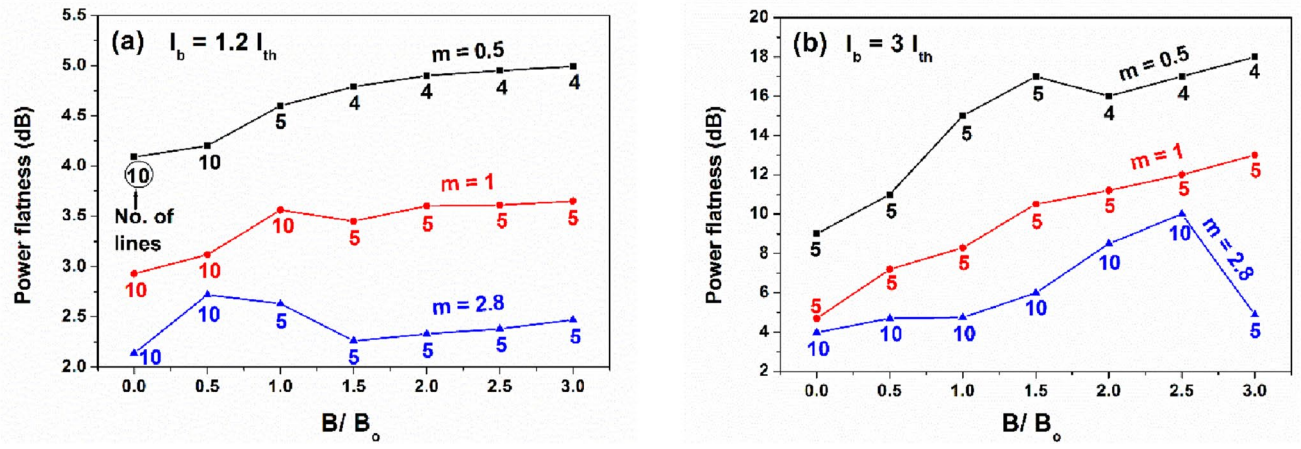

Fig. 7 Variation of numbers and power flatness of the generated comb lines as a function of B normalized to B_o under three distinct modulation depths of $m = 0.5$ (black line), 1 (red line) and 2.8 (blue line) when **a** $I_b = 1.2$ and **b** $3I_{th}$

of gain suppression and/or stronger modulation depth m. Comparing Fig. 7a, b reveals that when the laser is biased at $I_b = 1.2I_{th}$, the power flatness is lower and more acceptable (< 5 dB) than when biased at $I_b = 3I_{th}$. Moreover, the influence of gain suppression on the power flatness is weaker at $I_b = 1.2I_{th}$ than at $3I_{th}$. As a numerical example, when B increases from 0 to $3B_o$ at $m = 1$, the power flatness increases from 2.93 to 3.65 dB when $I_b = 1.2I_{th}$, whereas it increases from 4.7 to 13 dB when $I_b = 3I_{th}$. On the other hand, it can be noticed that the number of comb lines increases significantly when m increases from 1 to 2.8 at $I_b = 3I_{th}$ (large enough to avoid the total demise of stimulated emissions), which agree with the explanations reported in [11]. It can be concluded from the above discussions that the optimum conditions of generating OFCs (10 comb lines with power flatness of 2.1 dB) are at $B = 0$ and $m = 2.8$ when $I_b = 1.2I_{th}$.

Comprehensive details on influence of gain suppression on the width of the generated pulses are illustrated in Fig. 8a, b using the same parameters of Fig. 7a, b, respectively. The figures indicate that there is a pronounced broadening of the generated pulse width associated with increase of B and/or a decrease of m. Comparing Fig. 8a, b reveals that the pulses generated when $I_b = 1.2I_{th}$ are narrower than those generated when $I_b = 3I_{th}$. Moreover, the influence of gain suppression on the generated pulse width when $I_b = 1.2I_{th}$ is weaker than on those generated when $I_b = 3I_{th}$. As a numerical example, when B increases from 0 to $3B_o$ at $m = 1$, the FWHM of the pulses increases from 67 to 119 ps (increase of 52 ps) at $I_b = 1.2I_{th}$, whereas it increases from 169 to 291 ps (increase of 122 ps) when I_b rises to $3I_{th}$. This effect is more significant under week modulation depth of $m = 0.5$ (low populations) than under strong depth of $m = 2.8$ (high populations). The idea of broadening the emitted pulses with reduction of population pulsation agrees with the experimental results in [32].

4 Conclusions

We showed that it is possible to produce a route to OFCs of semiconductor laser by gain-switching method using the cost-effective technique of direct sinusoidal current modulation of semiconductor laser without need for external optical injection. We examined in details influence of nonlinear gain suppression on the temporal and frequency characteristics of the generated pulses and OFCs. The investigations were in terms of the relaxation oscillations, phase portrait, and small-signal modulation response for the non-modulated laser, and the temporal trajectories of electron and photon numbers and the FFT spectra for the generated OFCs. Based on the results obtained in the present study, conclusions can be itemized as follows:

(1) The damping rate of the laser relaxation oscillations increases with the increase of gain suppression coefficient B and/or I_b.
(2) The modulation response is reduced with the increase of B especially around the response peak. This effect is more robust at higher biasing current; when B increases from 0 to $3B_o$, the reduction is 0.6 dB when $I_b = 3I_{th}$, whereas it is 0.24 dB when $I_b = 1.2I_{th}$.
(3) The optimum parameters to generate a large number of comb lines with low-power flatness are low gain suppression along with stronger modulation depth m when the laser is biased near the threshold. Ten comb lines with power flatness of 2.1 dB are predicted at $B = 0$ and $m = 2.8$ when $I_b = 1.2I_{th}$. Increasing B to $3B_o$ and decreasing m to 0.5 results in significant reduction in the number of comb lines to 5 with a higher flatness of 4.99 dB. This effect is more significant when $I_b = 3I_{th}$ with high ranges of power flatness.

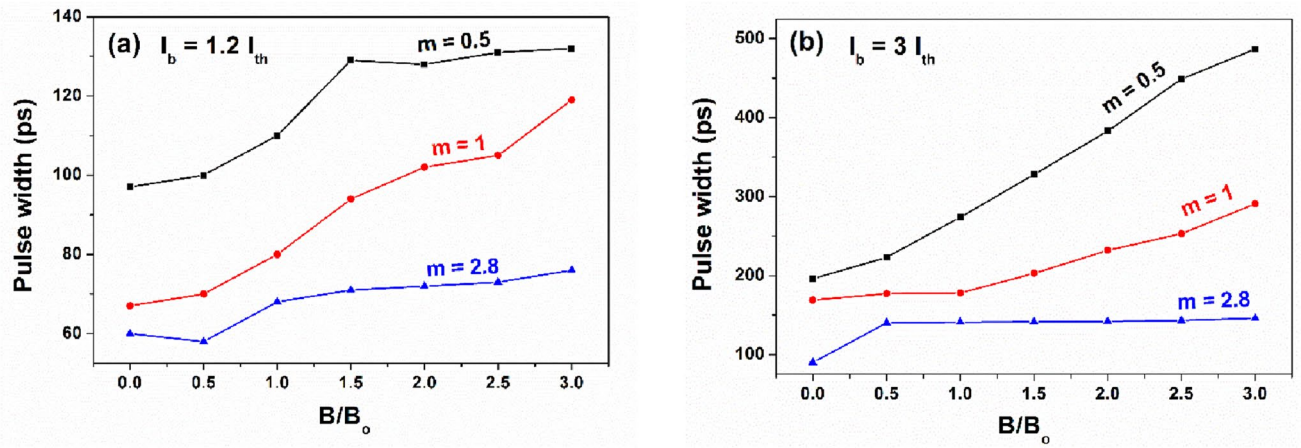

Fig. 8 Variation of the generated pule width as a function of B under three distinct modulation depths of $m = 0.5$ (black line), 1 (red line) and 2.8 (blue line) when **a** $I_b = 1.2$ and **b** $3I_{th}$

(4) The frequency spacing between comb lines (frequency repetition rate) increases by increasing the modulation frequency; the comb spacing increases from 1.35 to 4.45 GHz when the modulation frequency increases from 2.7 to 8.9 GHz, respectively.
(5) Generation of short pulses results when gain suppression is low and/or the modulation depth is strong when the laser is biased near the threshold. Pulses with 60 ps width are generated at $B=0$ and $m=2.8$ when $I_b=1.2I_{th}$. Increasing B to $3B_o$ and decreasing m to 0.5 induce a significant broadening of pulses to 132 ps. This effect is more significant when $I_b=3I_{th}$ with higher widsth.

Author contributions AM: conceptualization, validation, formal analysis, writing—original draft, visualization. MA: conceptualization, software, writing—review & editing, supervision.

Funding This research did not receive any specific grant from funding agencies in the public, commercial, or not-for-profit sectors.

Declarations

Conflict of interest The authors declare no conflicts of interest.

References

1. V. Torres-Company, A.J. Metcalf, D.E. Leaird, A.M. Weiner, Multichannel radio-frequency arbitrary waveform generation based on multiwavelength comb switching and 2-D line-by-line pulse shaping. IEEE Photonics Technol. Lett. **24**, 891–893 (2012)
2. V. Torres-Company, A.M. Weiner, Optical frequency comb technology for ultrabroadband radio-frequency photonics. Laser Photonics Rev. **8**, 368–393 (2014)
3. P. Peng, R. Shiu, M. Bitew, T. Chang, C. Lai, J. Junior, A 12 GHz wavelength spacing multi-wavelength laser source for wireless communication systems. Opt. Laser Technol. **93**, 175–179 (2017)
4. M. Imran, P.M. Anandarajah, A. Kaszubowska-Anandarajah, N. Sambo, L. Poti, A survey of optical carrier generation techniques for terabit capacity elastic optical networks. IEEE Commun. Surv. Tutor. **20**, 211–263 (2018)
5. Y. Yang, J. Ma, X. Xin, Q. Zhang, Y. Zhang, X. Yin, W. Liu, Optical frequency comb generation using two cascaded polarization modulators. Photonic Netw. Commun. **32**, 126–132 (2016)
6. R.B. Chaudhuri, A.D. Barman, Generation of an optical frequency comb based on two cascaded dual-parallel polarization modulators. Appl. Opt. **57**, 9164–9171 (2018)
7. J. Zhi, D.E. Leaird, C.B. Huang, H. Miao, M. Kourogi, K. Imai, A.M. Weiner, Spectral line-by-line pulse shaping on an optical frequency comb generator. IEEE J. Quantum Electron. **43**, 1163–1174 (2007)
8. S. Ozharar, F. Quinlan, I. Ozdur, S. Gee, P.J. Delfyett, Ultraflat optical comb generation by phase-only modulation of continuous wave light. IEEE Photonics Technol. Lett. **20**, 36–38 (2008)
9. S.L. Jansen, A.A. Amin, H. Takahashi, I. Morita, H. Tanaka, 132.2-Gb/s PDM-8QAM-OFDM transmission at 4-b/s/Hz spectral efficiency. IEEE Photonic Technol. Lett. **21**, 802–804 (2009)
10. P.M. Anandarajah, S.P.Ó. Dúill, R. Zhou, L.P. Barry, Enhanced optical comb generation by gain-switching a single-mode semiconductor laser close to its relaxation oscillation frequency. IEEE J. Sel. Top. Quantum Electron. **21**, 592–600 (2015)
11. A. Rosado, A. Perez-Serrano, J.M.G. Tijero, A. Valle, L. Pesquera, I. Esquivias, Experimental study of optical frequency comb generation in gain-switched semiconductor lasers. Opt. Laser Technol. **108**, 542–550 (2018)
12. P.M. Anandarajah, R. Maher, Y.Q. Xu, S. Latkowski, J. O'Carroll, S.G. Murdoch, R. Phelan, J. O'Gorman, L.P. Barry, Generation of coherent multicarrier signals by gain switching of discrete mode lasers. IEEE Photonics J. **3**, 112–122 (2011)
13. A. Rosado, A. Pérez-Serrano, J.M.G. Tijero, A.V. Gutierrez, L. Pesquera, I. Esquivias, Numerical and experimental analysis of optical frequency comb generation in gain-switched semiconductor lasers. IEEE J. Quantum Electron. **55**, 1–12 (2019)
14. H. Ren, L. Fan, N. Liu, Z. Wu, G. Xia, Generation of broadband optical frequency comb based on a gain-switching 1550 nm vertical-cavity surface-emitting laser under optical injection. Photonics **7**(4), 95 (2020)
15. I.L. Gheorma, G.K. Gopalakrishnan, Flat frequency comb generation with an integrated dual-parallel modulator. IEEE Photonics Technol. Lett. **19**, 1011–1013 (2007)
16. R. Wu, V.R. Supradeepa, C.M. Long, D.E. Leaird, A.M. Weiner, Generation of very flat optical frequency combs from continuous-wave lasers using cascaded intensity and phase modulators driven by tailored radio frequency waveforms. Opt. Lett. **35**, 3234–3236 (2010)
17. M. Dong, S.T. Cundiff, H.G. Winful, Physics of frequency-modulated comb generation in quantum-well diode lasers. Phys. Rev. A **97**, 053822 (2018)
18. M.W. Day, M. Dong, B.C. Smith, R.C. Owen, G.C. Kerber, T. Ma, S.T. Cundiff, Simple single-section diode frequency combs. APL Photonics **5**, 121303 (2020)
19. L.A. Sterczewski, C. Frez, S. Forouhar, D. Burghoff, M. Bagheri, Frequency-modulated diode laser frequency combs at 2 μm wavelength. APL Photonics **5**, 076111 (2020)
20. J. Hillbrand, D. Auth, M. Piccardo, N. Opačak, E. Gornik, G. Strasser, B. Schwarz, In-phase and anti-phase synchronization in a laser frequency comb. Phys. Rev. Lett. **124**, 023901 (2020)
21. J.B. Khurgin, Y. Dikmelik, A. Hugi, J. Faist, Coherent frequency combs produced by self-frequency modulation in quantum cascade lasers. Appl. Phys. Lett. **104**, 081118 (2014)
22. T. Shao, M. Beltrán, R. Zhou, P.M. Anandarajah, R. Llorente, L.P. Barry, 60 GHz radio over fiber system based on gain switched laser. J. Lightw. Technol. **32**, 3695–3703 (2014)
23. P.C. Peng, K.C. Shiu, Y.M. Chen, M.A. Bitew, W.Y. Lee, C.H. Lai, Y.W. Peng, Multiwavelength laser module based on distribute feedback laser diode for broadcast and communication systems. IEEE Photonics J. **8**, 1–8 (2014)
24. P.M. Anandarajah, R. Zhou, R. Maher, D. Lavery, M. Paskov, B. Thomsen, L.P. Barry, Gain-switched multicarrier transmitter in a long-reach UDWDM PON with a digital coherent receiver. Opt. Lett. **38**, 4797–4800 (2013)
25. B. Jerez, P. Martín-Mateos, E. Prior, C. de Dios, P. Acedo, Dual optical frequency comb architecture with capabilities from visible to mid-infrared. Opt. Express **24**, 14986–14994 (2016)
26. S.P.Ó. Dúill, R. Zhou, P.M. Anandarajah, L.P. Barry, Analytical approach to assess the impact of pulse-to-pulse phase coherence of optical frequency combs. IEEE J. Quantum Electron. **51**, 1–8 (2015)
27. H. Zhu, R. Wang, T. Pu, P. Xiang, J. Zheng, T. Fang, A novel approach for generating flat optical frequency comb based on

externally injected gains witching distributed feedback semiconductor laser. Laser Phys. Lett. **14**, 026201 (2017)
28. R. Zhou, P.M. Anandarajah, M.D.G. Pascual, J. O'Carroll, R. Phelan, B. Kelly, L.P. Barry, Monolithically integrated 2-section lasers for injection locked gain switched comb generation, in *Proceedings of OFC*, OSA, 2014, Th3A.3.
29. G. Arnold, P. Russer, Modulation behavior of semiconductor injection lasers. Appl. Phys. **14**, 255–268 (1977)
30. H. Kressel, J.K. Butler, *Semiconductor Lasers and Heterojunction LEDs, Chap. 17* (Academic, New York, 1977)
31. H. Ito, H. Yokoyama, S. Murata, H. Inaba, Picosecond optical pulse generation from an r.f. modulated AlGaAs d.h. diode laser. Electron. Lett. **15**, 738–740 (1979)
32. S. Tarucha, K. Otsuka, Response of semiconductor laser to deep sinusoidal injection current modulation. IEEE J. Quantum Electron. **17**, 810–816 (1981)
33. J. AuYeung, Picosecond optical pulse generation at gigahertz rates by direct modulation of a semiconductor laser. Appl. Phys. Lett. **38**, 308–310 (1981)
34. M. Ahmed, A. El-Lafi, Large-signal analysis of analog intensity modulation of semiconductor lasers. Opt. Laser Technol. **40**, 809–819 (2008)
35. D.J. Channin, Effect of gain saturation on injection laser switching. Appl. Phys. Rev. **50**, 3858–3860 (1979)
36. C.H. Henry, Theory of phase noise and power spectrum of a single mode injection laser. IEEE J. Quantum Electron. **19**, 1391–1397 (1983)
37. K.Y. Lau, Gain switching of semiconductor injection lasers. Appl. Phys. Lett. **52**, 257–259 (1988)
38. R.A. Abdullah, The influence of gain suppression on dynamic characteristics of violet InGaN laser diodes. Optik **125**, 580–582 (2014)
39. M.J. Adams, M. Osinski, Influence of spectral hole-burning on quaternary laser transients. Electron. Lett. **19**, 627–628 (1983)
40. J.E. Bowers, T.L. Koch, B.R. Hemenway, D.P. Wilt, T.J. Bridges, E.G. Burkhardt, High-frequency modulation of 1.52 μm vapour-phase-transported InGaAsP lasers. Electron. Let. **21**, 297–299 (1985)
41. K. Furuya, Y. Suematsu, T. Hong, Reduction of resonance like peak in direct modulation due to carrier diffusion in injection laser. Appl. Opt. **17**, 1949–1952 (1978)
42. B.N. Gomatam, A.P. DeFonzo, Gain suppression in semiconductor lasers: the influence of dynamic carrier temperature changes. J. Appl. Phys. **64**, 1555–1557 (1988)
43. C.Y. Tsai, R.M. Spencer, Y.H. Lo, L.F. Eastman, Nonlinear gain coefficients in semiconductor lasers: effects of carrier heating. IEEE J. Quantum. Electron. **32**, 201–212 (1996)
44. M. Ahmed, M. Yamada, S.W. Mahmoud, Analysis of semiconductor laser dynamics under gigabit rate modulation. J. Appl. Phys. **101**, 033119 (2007)
45. M. Ahmed, M. Yamada, An infinite order perturbation approach to gain calculation in injection semiconductor lasers. J. Appl. Phys. **84**, 3004–3015 (1998)
46. M. Ahmed, M. Yamada, Influence of instantaneous mode competition on the dynamics of semiconductor lasers. IEEE J. Quantum Electron. **38**, 682–693 (2002)
47. R.L. Burden, J.D. Faires, A.C. Reynolds, *Numerical Analysis*, 2nd edn. (Prindle, Boston, 1981). (**Weber and Schmidt**)
48. M. Ahmed, M. Yamada, Mode oscillation and harmonic distortions associated with sinusoidal modulation of semiconductor lasers. Eur. Phys. J. D **66**, 246 (2012)
49. K. Petermann, *Laser Diode Modulation and Noise* (Kluwer Academic, Dordrecht, 1988)
50. M. Ahmed, A. El-Lafi, Analysis of small-signal intensity modulation of semiconductor lasers taking account of gain suppression. Pramana **71**, 99–115 (2008)
51. S.W. Mahmoud, M.F. Ahmed, K. Abdelhady, A. Mahmoud, Estimation of parameters controlling direct modulation of semiconductor lasers, In: 2009 national radio science conference, IEEE, pp. 1–9
52. S.W.Z. Mahmoud, Influence of gain suppression on static and dynamic characteristics of laser diodes under digital modulation. Egypt. J Solids **30**, 237–251 (2007)
53. B. Zhao, T.R. Chen, A. Yariv, The gain and carrier density in semiconductor lasers under steady-state and transient conditions. IEEE J. Quantum electron. **28**, 1479–1486 (1992)
54. B. Lingnau, K. Lüdge, W.W. Chow, E. Schöll, Influencing modulation properties of quantum-dot semiconductor lasers by carrier lifetime engineering. Appl. Phys. Lett. **101**, 131107 (2012)
55. Y.C. Chen, H.G. Winful, J.M. Liu, Subharmonic bifurcations and irregular pulsing behavior of modulated semiconductor lasers. Appl. Phys. Lett. **47**, 208–210 (1985)
56. L. Chusseau, E. Hemery, J.M. Lourtioz, Period doubling in directly modulated InGaAsP semiconductor lasers. Appl. Phys. Lett. **55**, 822–824 (1989)
57. E. Hemery, L. Chusseau, J.M. Lourtioz, Dynamic behaviors of semiconductor lasers under strong sinusoidal current modulation: modeling and experiments at 13 μm. IEEE J. Quantum Electron. **26**, 633–641 (1990)